International Journal of Nanomedicine

Dovepress

open access to scientific and medical research

Open Access Full Text Article

ORIGINAL RESEARCH

Europium-Containing Nanospheres for Treating Ovariectomy-Induced Osteoporosis: Targeted Bone Remodeling and Macrophage Polarization Modulation

Yu-Chi Wang[1,*], Meng-Ting Cai[1,*], Ming-Hong Chen[2,3], Fu-I Tung[4,5], Mei-Hsiu Chen[6,7], Tse-Ying Liu[1]

[1]Department of Biomedical Engineering, National Yang Ming Chiao Tung University, Taipei, 112304, Taiwan; [2]Division of Neurosurgery, Department of Surgery, Far Eastern Memorial Hospital, New Taipei City, 220216, Taiwan; [3]Department of Electrical Engineering, Yuan Ze University, Taoyuan City, 320315, Taiwan; [4]Department of Orthopaedics, Yang-Ming Branch, Taipei City Hospital, Taipei, 111024, Taiwan; [5]Department of Health and Welfare, College of City Management, University of Taipei, Taipei, 111036, Taiwan; [6]Department of Internal Medicine, Far Eastern Memorial Hospital, New Taipei City, 220216, Taiwan; [7]Department of Biomedical Engineering, Ming Chuang University, Taoyuan, 333, Taiwan

*These authors contributed equally to this work

Correspondence: Tse-Ying Liu; Mei-Hsiu Chen, Email tyliu5@nycu.edu.tw; michelle8989@gmail.com

Purpose: Osteoporosis, characterized by reduced bone mass and structural deterioration, poses a significant healthcare challenge. Traditional treatments, while effective in reducing fracture risks, are often limited by side effects. This study introduces a novel nanocomplex, europium (Eu) ions-doped superparamagnetic iron oxide (SPIO) nanocrystals encapsulated in poly(lactic-co-glycolic acid) (PLGA) nanospheres, abbreviated as SPIO:Eu@PLGA nanospheres, as a potential therapeutic agent for osteoporosis by modulating macrophage polarization, enhancing osteoblast differentiation and inhibiting osteoclastogenesis.

Methods: SPIO and SPIO:Eu nanocrystals were synthesized through pyrolysis and encapsulated in PLGA using an emulsification method. To evaluate the impact of SPIO:Eu@PLGA nanospheres on macrophage reprogramming and reactive oxygen species (ROS) production, flow cytometry analysis was conducted. Furthermore, an ovariectomized (OVX) rat model was employed to assess the therapeutic efficacy of SPIO:Eu@PLGA nanospheres in preventing the deterioration of osteoporosis.

Results: In vitro, SPIO:Eu@PLGA nanospheres significantly attenuated M1 macrophage activation induced by lipopolysaccharides, promoting a shift towards the M2 phenotype. This action is linked to the modulation of ROS and the NF-κB pathway. Unlike free Eu ions, which do not achieve similar results when not incorporated into the SPIO nanocrystals. SPIO:Eu@PLGA nanospheres enhanced osteoblast differentiation and matrix mineralization while inhibiting RANKL-induced osteoclastogenesis. In vivo studies demonstrated that SPIO:Eu@PLGA nanospheres effectively targeted trabecular bone surfaces in OVX rats under magnetic guidance, preserving their structure and repairing trabecular bone loss by modulating macrophage polarization, thus restoring bone remodeling homeostasis. The study underscores the critical role of Eu doping in boosting the anti-osteoporotic effects of SPIO:Eu@PLGA nanospheres, evident at both cellular and tissue levels in vitro and in vivo.

Conclusion: The inclusion of Eu into SPIO matrix suggests a novel approach for developing more effective osteoporosis treatments, particularly for conditions induced by OVX. This research provides essential insights into SPIO:Eu@PLGA nanospheres as an innovative osteoporosis treatment, addressing the limitations of conventional therapies through targeted delivery and macrophage polarization modulation.

Keywords: osteoporosis, macrophage polarization, osteoblast, osteoclast, nanocrystals, poly(lactic-co-glycolic acid)

Introduction

Osteoporosis is a skeletal disease characterized by reduced bone mass, leading to increased risk of fractures.[1] It is divided into primary, often due to estrogen decline in post-menopausal women or aging in those over 75, and secondary, associated with various medical conditions and medications.[2,3] Predominantly affecting the elderly, osteoporosis poses

Received: 6 April 2024
Accepted: 26 September 2024
Published: 5 October 2024

a significant challenge as it remains asymptomatic until severe fractures occur. This leads to difficult treatments and potential lifelong confinement, increasing healthcare costs and reducing quality of life. Addressing osteoporosis treatment is thus crucial.

Osteoporosis is a condition characterized by an imbalance in bone remodeling, the continuous process of bone formation and resorption, leading to increased bone fragility and fracture risk.[4,5] Treatment strategies focus on inhibiting bone resorption (antiresorptive) or promoting bone formation (anabolic),[6,7] each with specific administration methods and potential side effects, such as osteonecrosis of the jaw and an elevated risk of cancer.[8–10] The complexity of managing osteoporosis highlights the need for innovative approaches to treatment, underpinned by a deeper understanding of bone metabolism. Recent research underscores the critical role of macrophages in bone remodeling, particularly their influence on the pathogenesis of osteoporosis.[11,12] Macrophages exist in various activation states, notably M1 and M2 phenotypes, which respond to different environmental cues and exhibit distinct functions. M1 macrophages, or classically activated macrophages, are known for their pro-inflammatory role and their contribution to increased bone resorption, partly by serving as precursors to osteoclasts.[13,14] In contrast, M2 macrophages, which arise in settings dominated by anti-inflammatory signals, are involved in tissue repair and remodeling.[15] The balance between these phenotypes is crucial for maintaining bone health, with shifts in the M1/M2 ratio being implicated in osteoporotic conditions.[16] Therefore, designing a strategy that targets osteoblasts, osteoclasts, and macrophages for treating osteoporosis is of great importance.

Our aim was to develop a biocompatible complex specifically designed for targeted delivery to bone tissue, capable of modulating macrophages, osteoblasts, and osteoclasts to regulate bone remodeling and address osteoporosis. In this study, we focused on developing superparamagnetic iron oxide (SPIO) nanocrystals, doped with europium (Eu) ions, encapsulated within poly(lactic-co-glycolic acid) (PLGA) to create SPIO:Eu@PLGA nanospheres. These nanospheres are ingeniously designed to influence bone remodeling actively. The SPIO nanocrystals perform several critical functions: they target specific bone sites through magnetically assisted delivery,[17] effectively scavenging reactive oxygen species (ROS).[18,19] The reduction of ROS may regulate the activation of macrophages, which, as previously mentioned, are pivotal in managing postmenopausal osteoporosis.[12,20] Additionally, the presence of Eu ions in bone is recognized for enhancing bone formation and promoting blood vessel growth,[21,22] making SPIO:Eu nanocrystals a potentially powerful agent for modulating macrophages and osteogenesis. This novel approach of using SPIO:Eu nanocrystals for osteoporosis treatment has not been previously reported. Moreover, research by Nicolete et al has shown that micro-scaled PLGA spheres can provoke strong inflammatory responses by binding to cell membranes, leading to the activation of nuclear factor kappa-light-chain-enhancer of activated B cells (NF-κB) and cytokine production.[23] In contrast, our pilot study demonstrated that nano-scaled PLGA spheres did not exhibit such effects, indicating a size-dependent inflammatory response. In addition, materials similar to PLGA have been widely utilized for their osteoconductivity and efficacy in bone repair, further supporting their role in facilitating bone regeneration processes.[24,25] Leveraging these findings, we used PLGA nanospheres to encapsulate the lipophilic SPIO:Eu nanocrystals, creating an injectable suspension formulation. Consequently, an intravenous (IV) injection formulation containing SPIO:Eu-embedded PLGA nanospheres (SPIO:Eu@PLGA) was developed to explore its effects on bone remodeling, which has yet to be examined thoroughly.

In this study, we prepared and characterized the SPIO:Eu@PLGA nanospheres, assessing their effectiveness in treating osteoporosis in ovariectomized (OVX) rats, and examining the underlying mechanisms, especially the immunomodulation of macrophage polarization on osteogenesis and osteoclastogenesis. This formulation aims to harness the therapeutic potential of nanotechnology for osteoporosis treatment, presenting a significant advancement in the field.

Materials and Methods

Material Preparation and Characterization Analysis

Iron (III) chloride hexahydrate (99%) was purchased by SHOWA. Sodium oleate (97%) was obtained by TCI. Europium (III) acetate hydrate (99.9%) was purchased by Alfa Aesar. Tri-n-octylamine was obtained by Thermo scientific. Oleic

acid, poly(D,L-lactide-co-glycolide) (Mw 7,000–17,000) and poly(vinyl alcohol) (87–90%) was purchased by Sigma-Aldrich.

Synthesis of SPIO and SPIO:Eu Nanocrystals

The iron oleate complex, a precursor for preparing SPIO and SPIO:Eu nanocrystals, was synthesized by reacting iron chlorides with sodium oleate. Iron (III) chloride hexahydrate (10 mmol), sodium oleate (3.33 mmol), 5 mL of distilled water, 6.6 mL of ethanol, and 11.67 mL of hexane were combined in a three-neck round-bottom flask. The mixture was heated to 70 °C and held at this temperature while stirring at 130 rpm for 4 h. Following the completion of the reaction, the upper layer, which contained the iron-oleate complex, underwent three washes with distilled water using a separatory funnel. Subsequent to the evaporation of hexane, a reddish-brown iron-oleate complex in the form of waxy solid was obtained.

Monodispersed hydrophobic SPIO:Eu nanocrystals were synthesized through thermal decomposition. A mixture containing iron oleate complex (3 mmol), synthesized as previously described, europium (III) acetate (0.1 mmol), and oleic acid (18 mmol; boiling point = 360 °C) was dissolved in tri-n-octylamine (16.6 g; boiling point = 365–367 °C) within a three-neck flask. The reaction mixture was heated at a constant rate of 3.8°C/min until it approached the set temperature of 370 °C under a nitrogen flow. During this process, a condenser was employed to ensure proper reflux and to prevent excessive vapor pressure buildup within the system. Upon nearing 370 °C, the mixture was maintained close to this temperature for 30 min. The yellow solution then underwent a vigorous reaction, turning black, indicating the formation of nanocrystals. After cooling to room temperature, 10 mL of ethanol was added to precipitate the nanocrystals. The precipitated SPIO:Eu nanocrystals were washed three times with ethanol, collected by centrifugation, and finally dispersed in hexane for subsequent use. The synthesis process for SPIO nanocrystals is similar to that of SPIO:Eu nanocrystals, except that europium (III) acetate was not added.

Preparation of SPIO@PLGA and SPIO:Eu@PLGA Nanospheres

Initially, SPIO:Eu nanocrystals (40 mg) was dispersed in dichloromethane (DCM) and combined with PLGA (40 mg) in a sample bottle, followed by the addition of 10 mL of 2% polyvinyl alcohol (PVA). The mixture was then subjected to ultrasonic homogenization for 5 min. Subsequently, it was placed on a hot plate and heated to 80°C to evaporate the DCM. After the evaporation process, which took about 1 h, the mixture was washed twice with distilled water. The SPIO:Eu@PLGA nanospheres were collected by centrifuging at 13,200 rpm for 20 min. The final product was resuspended in 1% sucrose solution and stored at −20°C for future use. Following this protocol, the preparation of SPIO@PLGA nanospheres was conducted in an identical manner to that of the SPIO:Eu@PLGA nanospheres. Initially, SPIO nanocrystals (40 mg) were dispersed in dichloromethane (DCM) and mixed with PLGA (40 mg) in a sample bottle. This mixture was then treated in the same way as the SPIO:Eu@PLGA nanospheres.

Characterization of SPIO, SPIO:Eu, SPIO@PLGA, and SPIO:Eu@PLGA

The morphologies of SPIO nanoparticles, SPIO:Eu nanoparticles, SPIO@PLGA nanospheres, and SPIO:Eu@PLGA nanospheres were examined via transmission electron microscopy (TEM; JEOL JEM-1400 Plus). Particle size was performed employing dynamic light scattering (DLS; Malvern ZS90). Phase dentification was accomplished using X-ray diffraction (XRD; Bruker, D2 Phaser). Composition analysis was conducted through X-ray photoelectron spectroscopy (XPS; Thermo Scientific, Theta Probe).

Cell Viability Test

Mouse osteoblast precursor MC3T3-E1 cell lines and mouse macrophage RAW 264.7 cell lines were purchased from American Type Culture Collection (ATCC). Mouse osteoblast precursor MC3T3-E1 cells (ATCC® CRL-2593™, Manassas, VA, USA) were grown in Alpha modified Eagle's minimum essential medium (α-MEM) containing with fetal bovine serum (FBS; 10%) and penicillin and streptomycin (PS; 1%) in an incubator (5% CO_2, 37 °C). The same culture atmosphere was used for the mouse macrophage RAW 264.7 cell lines (ATCC® TIB-71™, Manassas, VA, USA). Dulbecco's modified eagle medium (DMEM/High Glucose) was used as the culture medium and supplemented with fetal bovine serum (FBS; 10%) and penicillin-streptomycin (PS; 1%).

MC3T3-E1 and RAW 264.7 cells, seeded at densities of 5×10^4 and 2×10^5 cells per well, respectively, were cultured in 24-well plates under the aforementioned conditions for 24 h. Following three washes with phosphate-buffered saline (PBS), SPIO@PLGA and SPIO:Eu@PLGA nanospheres, at concentrations of 0, 62.5, 125, 500, and 1000 μg/mL, were added to the plates in FBS-containing medium and further incubated for 24 h. Subsequently, after PBS washes, 5% PrestoBlue™ Cell Viability Reagent was introduced and allowed to react with the cells for 30 min. Viable cells were assessed by transferring 100 μL of supernatant to 96-well plates and measuring using an ELISA Reader (TECAN, infinite® 200 PRO, Zurich, Switzerland) with excitation/emission (Ex/Em) wavelengths set at 560/590 nm.

Macrophage Polarization and Nanospheres Treatment

RAW 264.7 macrophages from mice were seeded onto 6-well plates at a concentration of 2.5×10^5 cells per well and cultured for 24 h. Macrophage polarization was achieved by supplementation with lipopolysaccharides (LPS, MedChemExpress) 100 ng/mL and incubated for 24 h. After polarization into M1 macrophages, cells were incubated with SPIO@PLGA nanospheres (1 mg/mL), SPIO:Eu@PLGA nanospheres (1 mg/mL), and $Eu(CH_3COO)_3$ (0.2 mg/mL) for 24 h. $Eu(CH_3COO)_3$ was used as a comparison group to validate the specificity of the effects attributed to Eu ions when incorporated into the SPIO crystal matrix.

Flow Cytometry Analysis

Following polarization with LPS and the various treatments outlined above, the cells in the 6-well plates were rinsed with PBS. Trypsin was then employed to detach the cells. Subsequently, the cell lysate (1×10^6 cells) was transferred to a 1 mL Eppendorf tube and centrifuged at 1000 rpm for 5 min.

Measurement of M1 and M2 Macrophage Cell Surface Markers

Upon removal of the supernatant, cells were conjugated with fluorescein isothiocyanate (FITC)-labeled anti-mouse CD11c antibody (BioLegend) and Allophycocyanin (APC)-labeled anti-mouse CD163 antibody (BioLegend). Fc receptors were blocked using TruStain FcXTM (anti-mouse CD16/32) antibody obtained from BioLegend. A Beckman Coulter CytoFLEX Flow Cytometer (Beckman Coulter Inc., Brea, CA, USA) was employed to analysis M1 and M2 macrophages.

Intracellular ROS Detection

After centrifugation and removal of the supernatant, the cells were exposed to a mixture of 1 μL of CellROX™ Deep Red Reagent and 99 μL of PBS in a dark environment for 30 min. Subsequently, after PBS rinses, the cells were suspended in 1 μL of medium and analyzed using flow cytometry (Beckman Coulter CytoFLEX, Beckman Coulter Inc., Brea, CA, USA) to measure the fluorescence intensity of ROS at excitation/emission wavelengths of 495/529 nm.

Western Blot

After a 24-hour treatment period, cells underwent three washes with PBS before being lysed in buffer for 5 minutes. The protein concentration in each cell lysate was determined and adjusted accordingly. Subsequently, proteins were isolated through the use of sodium dodecyl sulfate polyacrylamide gel electrophoresis (SDS-PAGE), followed by a transferred process onto a polyvinylidene fluoride (PVDF) membrane. The PVDF membranes were then put in a blocking solution containing 5% bovine serum albumin (BSA). It was then followed by incubation (4 °C) with the respective primary antibodies (phosphorylated NF-κB, p-NF-κB, Cell Signaling 3033S). After overnight incubation and washing, the PVDF membranes were incubated with the secondary antibodies (β-actin, GTX109639) at 4°C for 2 h and subsequently washed by PBS. Finally, the membranes were visualized using a luminescence/fluorescence imaging system (Amersham Imager-600/680), and the bands were recorded.

Osteoclastogenesis and Osteoblastogenesis

TRAP Staining

In the osteoclastogenesis experiments, RAW 264.7 cells were cultured to stimulate the development of multinucleated osteoclasts by employing macrophage colony-stimulating factor (M-CSF) and receptor activator of nuclear factor kappa-B ligand (RANKL). Multinucleated osteoclasts were identified through tartrate-resistant acid phosphatase (TRAP) staining and visualization of filamentous actin (F-actin). An osteoclastogenic supplement was prepared by adding 50 ng of RANKL and 30 ng of M-CSF to 1 mL of DMEM supplemented with 10% FBS and 1% PS. A total of 1×10^4 RAW 264.7 cells were seeded in a 12-well plate. The following day, after cell adherence, treatments with SPIO@PLGA (1 mg/mL), SPIO:Eu@PLGA (1 mg/mL), and $Eu(CH_3COO)_3$ (0.2 mg/mL) were initiated, with the osteogenic culture medium being refreshed every 2–3 days. Control groups included a negative control (NC, cells not treated with RANKL and M-CSF) and a positive control (PC, cells treated solely with RANKL and M-CSF). $Eu(CH_3COO)_3$ served as a comparison group to validate the specificity of the effects attributed to Eu ions when incorporated into the SPIO crystal matrix.

Following seven days of osteoclastogenesis induction and treatment with nanospheres as previously described, 12-well culture plates were washed three times with PBS and fixed with 1 mL of 4% formaldehyde for 20 min. After fixing, the plates were washed another three times with PBS. Each well then received 0.5 mL of TRAP reagent (TRAP Staining Kit, COSMO BIO) and was stained for up to 1 h. After staining, wells were thoroughly rinsed with water and observed under a microscope.

F-Actin Staining

Immerse the 18 mm circular slide in 99% alcohol, and carefully dry the surface of the slide using an alcohol lamp. Then, place the treated slide into a 12-well plate. Subsequently, seed 1×10^4 MC3T3-E1 cells onto the circular slide. Finally, allow the cells to attach by waiting for 24 h. Following the induction of osteoclastogenesis and treatment with nanospheres as described above for 7 days, the slides were collected and rinsed three times with PBS. Subsequently, they were fixed with 1 mL of 4% formaldehyde for 20 min, followed by three additional washes with PBS. Adding 1mL 0.1% Triton X-100 and incubate for 10 min. After washing with PBS, F-actin was stained with Alexa Fluor™ 568 Phalloidin (Invitrogen) for 1 h. The circular slides were mounted with 4',6-diamidino-2-phenylindole (Fluoroshield™ with DAPI, GeneTex) on glass slides and observed by an upright fluorescence microscope. (Leica, DM6000B; Ex/Em 405/594 nm, Magnification/Numerical Aperture 63×/1.4, red-orange fluorescence for F-actin).

Alkaline Phosphatase (ALP) Activity Assay

For osteoblastic differentiation experiments, culture medium with osteogenic supplement was prepared first by adding 2 mg L-ascorbic acid (Sigma-Aldrich; Merck KGaA) and 68.8 mg β-glycerophosphate disodium salt hydrate (Sigma-Aldrich; Merck KGaA) into 40 mL α-MEM with 10% FBS and 1% PS. In total, 5×10^4 MC3T3-E1 cells were seeded in a 12-well plate. The next day, when cells were attached to the plates, SPIO@PLGA (1 mg/mL), SPIO;Eu@PLGA (1 mg/mL), and $Eu(CH_3COO)_3$ (0.2 mg/mL) were added, and we replaced the osteogenic culture medium every 2–3 days. $Eu(CH_3COO)_3$ was used as a comparison group to validate the specificity of the effects attributed to Eu ions when incorporated into the SPIO crystal matrix.

ALP activity was evaluated on days 7 and 14 post-treatment employing a commercially available ALP Assay kit (Abcam). In brief, following rinsing with ice-cold PBS, 1×10^5 cells were lysed in 100 µL of ALP assay buffer on ice and subsequently centrifuged at 13,200 rpm for 15 min at 4 °C. The supernatant (80 µL) from each sample was then transferred into a 96-well plate and combined with 50 µL of 5 mm pNPP solution. This mixture was incubated at 25 °C in the absence of light for 60 min. The alkaline phosphatase activity was determined by assessing the absorbance at 405 nm utilizing an ELISA Reader (TECAN, infinite® 200 PRO, Zurich, Switzerland).

Alizarin Red S Staining for Mineral Deposition

Mineral deposition was evaluated on day 21 post-treatment utilizing Alizarin Red S Staining (Merck KGaA). Initially, cells were thrice rinsed with phosphate buffered saline solution and followed by fixation with formaldehyde (4%) for 20 min. Subsequent to fixation, the cells underwent three washes with distilled water (ddH_2O) and were subsequently

subjected to staining with 40 mm Alizarin Red S for 30 min. Upon ddH_2O washing and air-drying, a light microscope (Leica, DM6000B, Germany) was used to obtain the images of the cells with mineral deposition.

In vivo Efficacy

OVX-Induced Osteoporosis Animal Model and Treatment with Nanospheres

Six- to eight-week-old female Sprague-Dawley (SD) rats were procured from the Laboratory Animal Center of National Yang Ming Chiao Tung University (NYCU). All experimental procedures involving animals were conducted in accordance with protocols approved by the Institutional Animal Care and Use Committee of National Yang Ming Chiao Tung University (NYCU-IACUC 1100514), ensuring proper treatment and housing conditions.

A 2 cm incision along the midline was made to separate the skin from the underlying fascia. Moving 1 cm laterally from the midline, another incision was created through the fascia. With careful dissection, the tissue was spread laterally, keeping it as superficial as possible until reaching the abdominal cavity. Tweezers were then used to gently extract the adipose tissue surrounding the ovary, allowing for its identification. The uterine horns and vessels were tied off 0.5–1 cm above the ovary, which was then removed along with the ligated adipose tissue before returning the remaining tissue into the abdominal cavity. This process was repeated on the opposite side. Wounds were closed preferably with a monofilament suture, and the animals were allowed to recover from anesthesia. Osteoporosis was induced in OVX rats one month post-operation. Treatment with SPIO@PLGA or SPIO:Eu@PLGA nanospheres (25 mg/kg) was administered intravenously twice a week for two months. All OVX and sham-operated rats were euthanized at 15 weeks of age.

Histological Examination by Hematoxylin-Eosin, and Goldner's Trichrome Staining

The femurs were initially fixed in 4% formaldehyde for a duration of seven days, followed by decalcification in 10% ethylenediaminetetraacetic acid (pH 7.4) for an additional seven days. Subsequently, the samples underwent dehydration and were embedded in paraffin. Slices were then obtained from the paraffin-embedded sections and subjected to staining with hematoxylin–eosin (HE), as well as Goldner's trichrome for collagen and iron deposit visualization.

Analysis of Inducible Nitric Oxide Synthase (iNOS) Expression in Bone Tissue

The evaluation of iNOS expression in bone tissue was conducted through Western blot analysis. Proteins were extracted from the bone tissue and subjected to the Western blot process. The samples underwent sequential incubation with primary antibodies (iNOS, GTX130246) and secondary antibodies (β-actin, GTX109639). Subsequently, the samples were observed using the luminescence/fluorescence imaging system (Amersham Imager-600/680).

Statistical Analysis

Prism software (Version 8, GraphPad Software, Inc., CA) was employed for data analysis. Each experiment was repeated independently a minimum of three times. Graphical representation of data shows the mean values with error bars indicating the standard deviation (SD). Statistical significance among groups was determined using analysis of variance (ANOVA), followed by multiple comparisons. A p-value less than 0.05 was considered statistically significant.

Results

Material Characterization of SPIO, SPIO:Eu, SPIO@PLGA, and SPIO:Eu@PLGA

Pristine SPIO and Eu-doped SPIO (SPIO:Eu) nanocrystals were synthesized via a pyrolysis method.[26,27] Their morphologies and particle sizes were characterized using TEM and DLS, respectively. Both SPIO and SPIO:Eu nanocrystals displayed an average particle size of 15±2 nm. Notably, pristine SPIO particles were spherical in shape, whereas doping them with Eu led to a cubic morphology (Figure 1a and b). XPS analysis was performed to further confirm the successful doping of Eu into SPIO nanocrystals (Figure S1). Additionally, phase identification for SPIO and SPIO:Eu nanocrystals was conducted using XRD, as shown in Figure 1e. According to JCPDs Card No. 26–1136, diffraction peaks corresponding to the (311), (222), (400), and (440) planes of the cubic spinel structure, indicative of magnetite, were observed in both SPIO and SPIO:Eu samples. Together, these results demonstrate the successful synthesis of SPIO and

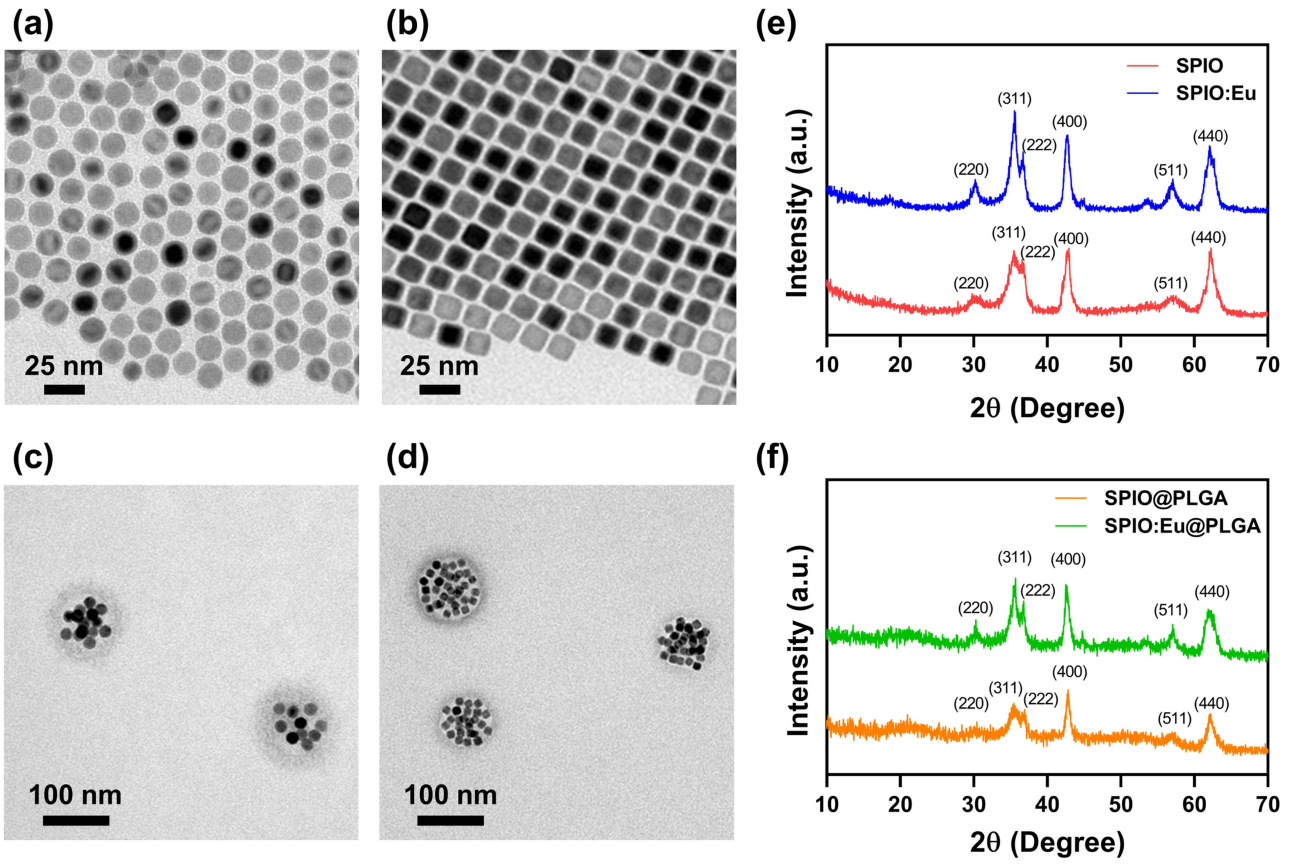

Figure 1 Transmission electron microscopy (TEM) images of (**a**) superparamagnetic iron oxide (SPIO) nanocrystals; (**b**) europium-doped SPIO (SPIO:Eu) nanocrystals; (**c**) SPIO nanocrystals embedded in poly(lactic-co-glycolic acid) nanospheres (SPIO@PLGA); and (**d**) SPIO:Eu nanocrystals embedded in PLGA nanospheres (SPIO:Eu@PLGA). X-ray diffraction (XRD) patterns of (**e**) SPIO and SPIO:Eu nanocrystals; and (**f**) SPIO@PLGA and SPIO:Eu@PLGA nanospheres. SPIO nanocrystal was successfully synthesized, retaining its crystal structure (phase) even after doping with Eu, despite the change in morphology. Following incorporation with PLGA, the crystal structures of both SPIO and SPIO:Eu nanocrystals remained consistent. The particle sizes for both SPIO@PLGA and SPIO:Eu@PLGA nanospheres were measured to be 90±10 nm.

SPIO:Eu nanocrystals, the doping of Eu into the SPIO nanocrystals, and the preservation of their crystal structure post-Eu doping.

To improve hydrophilicity for IV injectable formulation, PLGA was employed to encapsulate the hydrophobic SPIO and SPIO:Eu nanocrystals using an emulsification method. The resulting particle sizes for SPIO@PLGA and SPIO:Eu@PLGA nanospheres were both 90±10 nm. TEM images (Figure 1c and d) and XRD patterns (Figure 1f) confirmed the successful encapsulation of SPIO and SPIO:Eu nanocrystals within PLGA nanospheres.

In vitro Safety of SPIO:Eu@PLGA Nanospheres on Osteoblasts and Macrophages

Given that SPIO nanocrystals are FDA-approved as a magnetic resonance imaging (MRI) contrast agent, their safety for eukaryotic cells has been well established. In our study, we evaluated the cytotoxicity of SPIO@PLGA and SPIO:Eu@PLGA nanospheres using MC3T3-E1 cell lines, which are murine calvarial pre-osteoblasts commonly used in bone research. Additionally, we assessed their toxicity towards RAW264.7 (osteoclast precursors) cell lines, extensively employed in studies of osteoclastic differentiation, biological molecular mechanisms, and macrophage polarization. Remarkably, even at a high concentration of 1000 μg/mL, SPIO@PLGA and SPIO:Eu@PLGA nanospheres showed no significant toxicity towards either MC3T3-E1 or RAW264.7 cells, as depicted in Figure 2. Moreover, to further confirm the safety of SPIO@PLGA and SPIO:Eu@PLGA nanospheres in an intravenous dosage form, we conducted hemocompatibility tests (Figure S2), which demonstrated that neither formulation induced hemolysis, even at concentrations as high as 1000 μg/mL. Consequently, we chose a treatment dose of 1000 μg/mL for subsequent experiments.

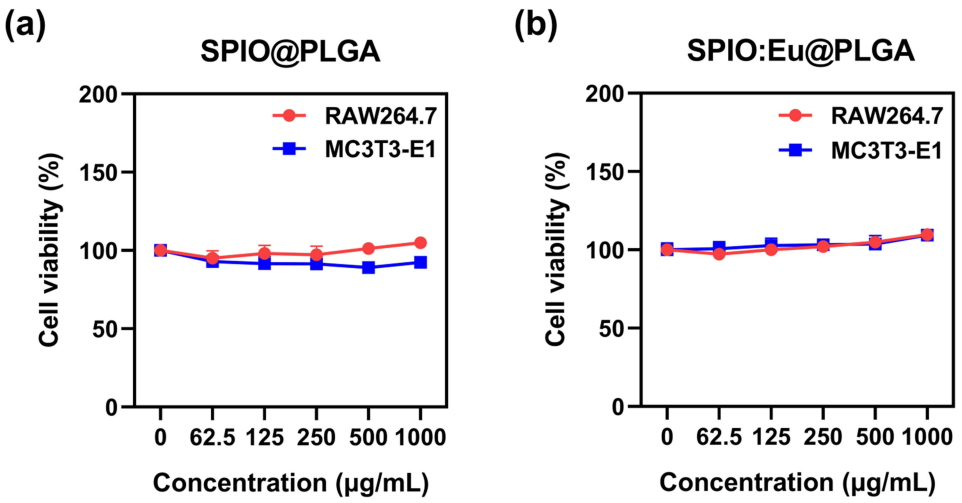

Figure 2 Effects of (**a**) SPIO@PLGA, and (**b**) SPIO:Eu@PLGA on the viability of MC3T3-E1 and RAW264.7 cells. Notably, even at a high concentration of 1000 μg/mL, the SPIO:Eu@PLGA nanospheres exhibited no significant toxicity towards both MC3T3-E1 and RAW264.7 cells after 24 h of incubation.

Effect of SPIO:Eu@PLGA Nanospheres on LPS-Induced M1 Macrophage Reprogramming

This study aimed to observe the effects of SPIO:Eu@PLGA nanospheres on LPS-induced M1 macrophage reprogramming through flow cytometry analysis. In addition, $Eu(CH_3COO)_3$ was used as a comparison group to validate the specificity of the effects attributed to Eu ions when incorporated into the SPIO nanocrystals. After the addition of LPS (100 ng/mL) to macrophages for one day, transforming them from the M0 phenotype to the M1 phenotype, SPIO@PLGA, SPIO:Eu@PLGA nanospheres and $Eu(CH_3COO)_3$ were co-cultured separately with these M1 phenotype macrophages. $CD11c^+$ is a protein expressed on M1 macrophages, while $CD163^+$ is expressed on M2 macrophages. As shown in Figure 3, following the induction of macrophages with LPS, the $CD11c^+/CD163^+$ ratio was markedly elevated (ie, polarization towards the M1). However, upon the addition of the prepared materials, there was a significant decrease in this expression ratio. Notably, SPIO:Eu@PLGA nanospheres exhibited the lowest $CD11c^+/CD163^+$ ratio, suggesting that SPIO:Eu@PLGA nanospheres can significantly suppress M1 expression, facilitating reprogramming and polarization towards the M2 phenotype.

Effects of SPIO:Eu@PLGA Nanospheres on ROS Production and the p-NF-κB Signaling Pathway in LPS-Induced M1 Macrophages

Upon classical activation by lipopolysaccharide (LPS), mouse RAW264.7 macrophages are polarized towards the M1 phenotype, characterized by the expression of iNOS. The upregulation of iNOS is known to be mediated by NF-κB,[28] with its activated state, p-NF-kB, believed to be linked to the intracellular levels of ROS.[29] By employing flow cytometry, we measured the intracellular ROS levels and observed that LPS-induced polarization towards M1 macrophages was associated with an increase in intracellular ROS (Figure 4a and b). Our results show that both SPIO@PLGA and SPIO:Eu@PLGA nanospheres inhibited intracellular ROS production, with SPIO:Eu@PLGA nanospheres demonstrating a more pronounced ROS scavenging ability compared to SPIO@PLGA nanospheres. Furthermore, as illustrated in Figure 4c, investigation into the transcription levels revealed that the expression of p-NF-κB was significantly reduced following treatment with both SPIO@PLGA and SPIO:Eu@PLGA nanospheres. Notably, the expression level of p-NF-κB induced by SPIO:Eu@PLGA nanospheres was lower than that induced by SPIO@PLGA nanospheres.

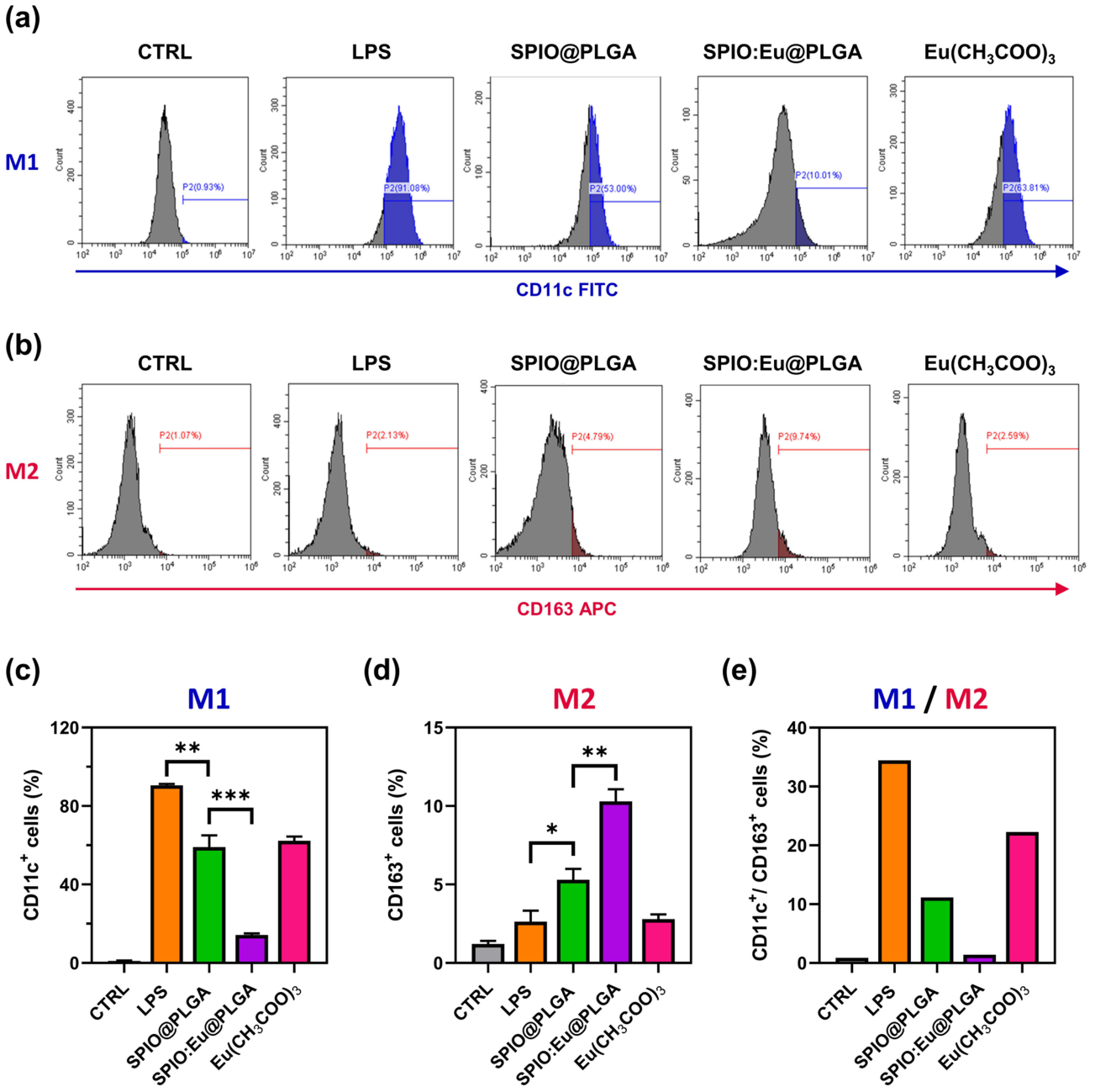

Figure 3 Effect of SPIO@PLGA and SPIO:Eu@PLGA nanospheres on macrophage polarization towards (**a**) M1 and (**b**) M2 in vitro, characterized by flow cytometry. (**c** and **d**) Quantitative and statistical analysis for (a) and (**b**), respectively. (**e**) The ratio of $CD11c^+/CD163^+$ (M1/M2). Notably, SPIO:Eu@PLGA nanospheres exhibited the lowest $CD11c^+/CD163^+$ ratio, suggesting that SPIO:Eu@PLGA nanospheres can significantly suppress M1 expression, facilitating reprogramming and polarization towards the M2 phenotype. $Eu(CH_3COO)_3$ was used as a comparison group to validate the specificity of the effects attributed to Eu ions when incorporated into the SPIO nanocrystals. Data represent the mean ± standard deviation from triplicate experiments. Statistical analysis was performed using one-way ANOVA (*p<0.05, **p<0.01 and ***p< 0.001).

Effect of SPIO:Eu@PLGA Nanospheres on Inhibiting RANKL-Induced Osteoclastogenesis

Osteoclasts exhibit several unique features for identification. First, they are multinucleated, a characteristic that can be identified using TRAP staining. Second, they possess distinctive cytoskeletons, ruffled membranes, and F-actin rings, enabling them to polarize on bone and degrade mineralized matrix. The F-actin ring, encircling the ruffled membrane, acts as a barrier to isolate the acidified resorptive microenvironment. This structure can be visualized using fluorescent and biotinylated phalloidin. In our study, osteoclastogenesis was induced in RAW264.7 cells with RANKL and M-CSF,

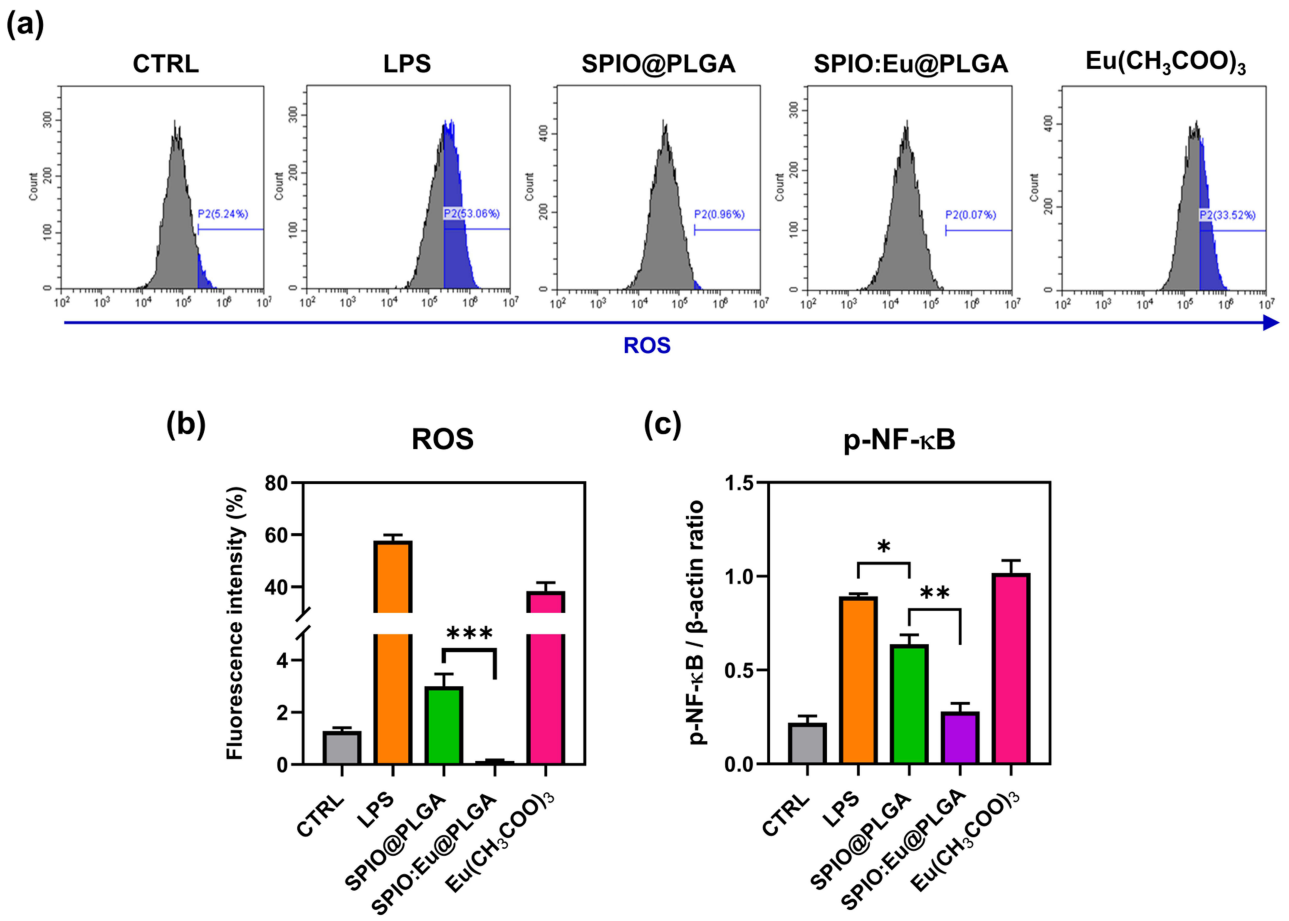

Figure 4 (**a**) Effects of SPIO@PLGA and SPIO:Eu@PLGA nanospheres on reactive oxygen species (ROS) production in LPS-induced M1 macrophages, characterized by flow cytometry. (**b**) Quantitative and statistical analysis of the data shown in panel (**a**). (**c**) Effects of SPIO@PLGA and SPIO:Eu@PLGA nanospheres on the phosphorylation of nuclear factor kappa-light-chain-enhancer of activated B cells (p-NF-κB) signaling pathway, characterized by Western blot. The treatment with SPIO:Eu@PLGA nanospheres resulted in a significant inhibition of both ROS and p-NF-κB production in LPS-induced M1 macrophages. Data represent the mean ± standard deviation from triplicate experiments. Statistical analysis of (**b**) was performed using a two-sided *t*-test, with statistical significance indicated as ***p<0.001. Statistical analysis of (c) was performed using one-way ANOVA (*p<0.05 and **p<0.01).

and observed after seven days. Notably, TRAP staining was significantly reduced in cells treated with SPIO@PLGA nanospheres, and more markedly with SPIO:Eu@PLGA nanospheres, as depicted in Figure 5a and b. Similarly, the formation of F-actin rings, indicated by white arrows in the F-actin staining images of the PC and $Eu(CH_3COO)_3$ groups, was impeded in cells treated with SPIO@PLGA nanospheres, particularly in those treated with SPIO:Eu@PLGA nanospheres, as evidenced in Figure 5c.

Effect of SPIO:Eu@PLGA Nanospheres on Osteoblasts Differentiation and Matrix Mineralization

In our study, MC3T3-E1 mouse pre-osteoblasts were utilized to evaluate osteoblast differentiation and matrix mineralization in vitro. We used ALP, a widely recognized biochemical marker of osteoblast activity, as an indicator. As indicated in Figure 6a, we noted that SPIO:Eu@PLGA nanospheres might hinder early osteoblast differentiation on day 7, yet both SPIO@PLGA and SPIO:Eu@PLGA nanospheres showed slight positive effects on osteoblast differentiation by day 14. Notably, ALP activity was significantly elevated on day 14 following treatment with SPIO:Eu@PLGA nanospheres. Bone mineralization, a critical process for new bone formation, is mediated by osteoblasts and involves embedding calcium phosphate nanocrystals into the organic bone matrix. In addition to assessing osteoblast differentiation, we evaluated matrix mineralization using Alizarin Red S staining on MC3T3-E1 cultures treated with our

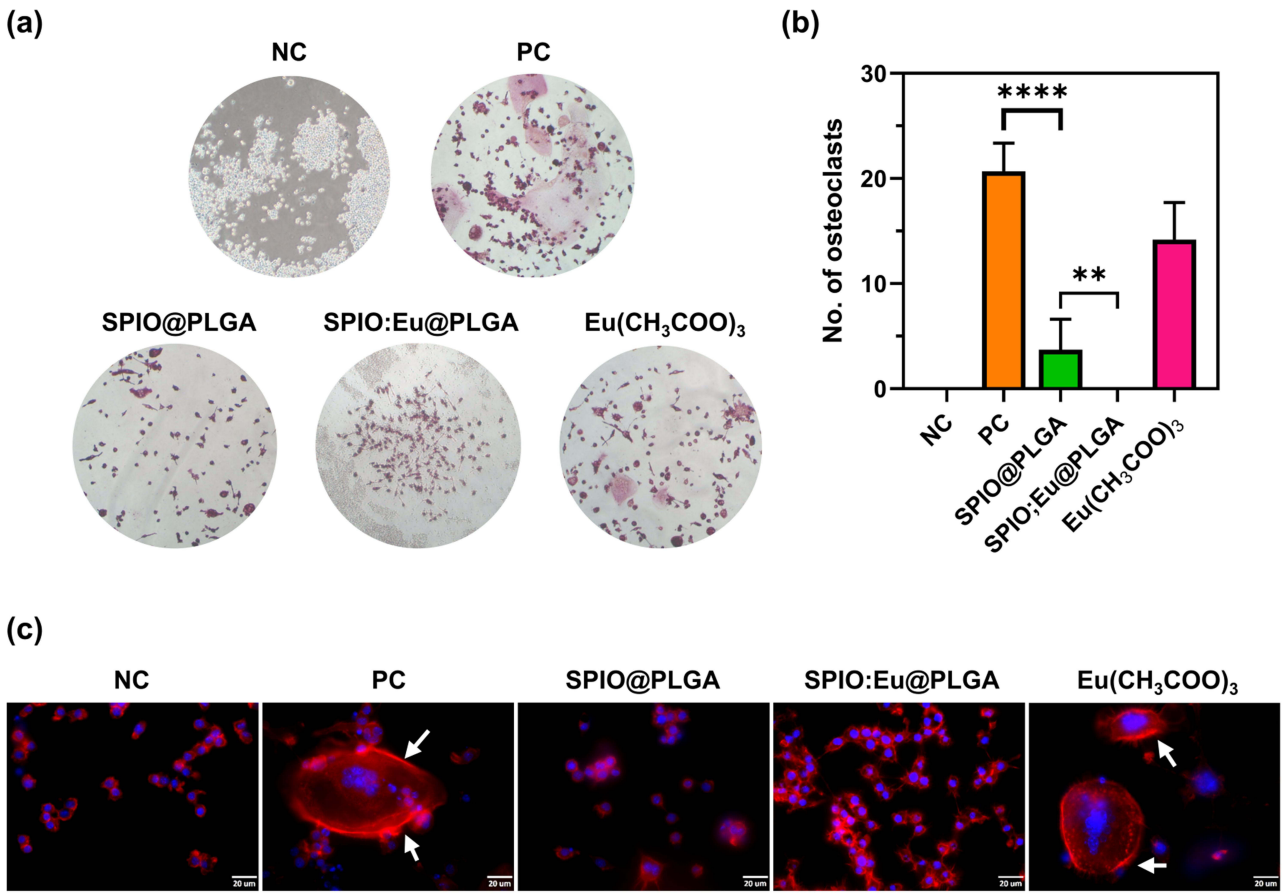

Figure 5 Effects of SPIO@PLGA and SPIO:Eu@PLGA nanospheres on inhibiting receptor activator of nuclear factor-κB ligand (RANKL)-induced osteoclastogenesis. (**a**) Characterization using tartrate-resistant acid phosphatase (TRAP) staining. (**b**) Quantitative and statistical analysis of the data presented in panel (**a**). (**c**) Evaluation based on the formation of filamentous actin (F-actin) rings, identified using fluorescent dye-labeled phalloidin. Scale bar: 20 μm. NC: negative control; PC: positive control. Notably, cells treated with SPIO:Eu@PLGA nanospheres showed a significant reduction in TRAP staining. Additionally, there was an impediment in the formation of F-actin rings, as indicated by white arrows in the images of F-actin staining in the PC and $Eu(CH_3COO)_3$ groups. Quantitative measurements of the images in this figure were conducted using ImageJ software. Data represent the mean ± standard deviation from triplicate experiments. Statistical analysis was performed using one-way ANOVA (**p<0.01 and ****p<0.0001).

nanospheres. Figure 6b shows that treatment with SPIO:Eu@PLGA nanospheres resulted in a marked increase in bone mineralization, as evidenced by the enhanced red staining observed after 21 days.

Effect of SPIO:Eu@PLGA Nanospheres on Preventing Deterioration of Osteoporosis in OVX-Rat

The in vivo therapeutic efficacy of SPIO:Eu@PLGA nanospheres was evaluated through an OVX-rat model. $Eu(CH_3COO)_3$ did not demonstrated the effect on M1 macrophage reprogramming and osteoblast differentiation; thus, it was excluded from the in vivo experiment. In addition, the localization of iron-containing SPIO nanocrystals was confirmed using Perls' Prussian Blue staining, which highlighted the accumulation of these nanoparticles in the bone marrow near the trabecular bone surface, as indicated by arrows in Figure S3.

Histological examination of femurs from OVX rats revealed contracted and perforated bone trabeculae, leading to disrupted continuity. This structural change was associated with a decrease in bone trabecular mass and an increase in bone marrow fat fraction. Figure 7a and b, analyzed using ImageJ software under light microscopy, show the trabecular area (ie, pink color in Figure 7a) measurements. These figures indicate that SPIO:Eu@PLGA nanospheres were most effective in preserving trabecular bone in the femurs of OVX rats. SPIO@PLGA also demonstrated a mild effect in preserving trabecular bone. In addition, Goldner's trichrome staining was employed to investigate trabecular content,

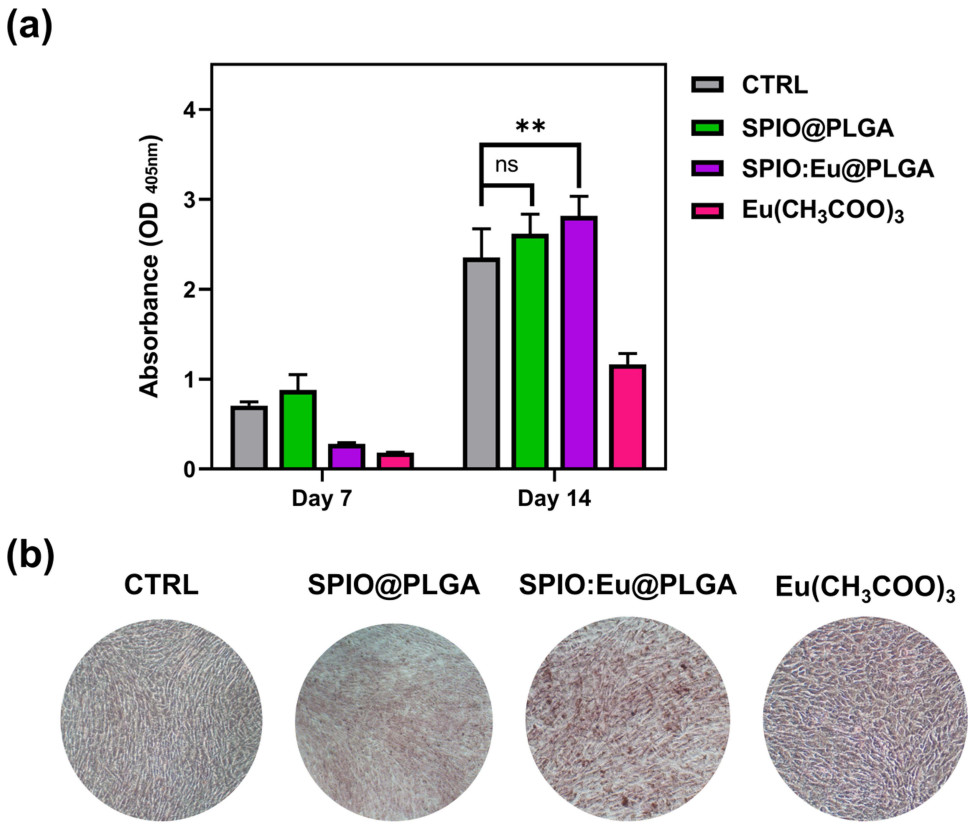

Figure 6 (**a**) Effects of SPIO@PLGA and SPIO:Eu@PLGA nanospheres on MC3T3-E1 osteoblast differentiation, characterized by alkaline phosphatase (ALP) assay. (**b**) Effects of SPIO@PLGA and SPIO:Eu@PLGA nanospheres on calcium deposition (ie, mineralization) at late osteogenesis of MC3T3-E1 cells, characterized by Alizarin Red S staining. Positive Alizarin Red S staining for calcium deposition was observed on day 21. Following treatment with SPIO:Eu@PLGA nanospheres, there was a notable elevation in ALP activity on day 14, along with a significant increase in the intensity of red staining, indicative of bone mineralization, observed on day 21. Data represent the mean ± standard deviation from triplicate experiments. Statistical analysis was conducted using one-way ANOVA (**p<0.01). The ns indicates no statistically significant differences (p > 0.05).

revealing that in osteoporotic femurs, trabeculae not only lost quantity but also their collagen content (ie, blue color in Figure 7c) in the bone matrix, which was replaced by non-mineralized content on the surface, with empty spaces in the central areas. As depicted in Figure 7c and d, the decrease in both the quantity and quality of trabeculae in OVX femurs could be mitigated by treatment with SPIO@PLGA nanospheres, and to an even greater extent with SPIO:Eu@PLGA nanospheres.

Histological analyses provide insights at the microscopic level, while micro-CT imaging further supports these findings on a larger scale. The representative cross-sectional images of micro-CT scans further supports these histological findings, demonstrating significant improvements in trabecular density, connectivity, and thickness in the SPIO:Eu@PLGA-treated group compared to the OVX and SPIO@PLGA groups (Figure S4; red arrows). The micro-CT images show that treatment with SPIO:Eu@PLGA nanospheres led to better preservation of trabecular structure, approaching that of the Sham group, while the OVX group exhibited considerable trabecular loss and disconnection.

Effect of SPIO:Eu@PLGA Nanospheres Treatment on OVX-Induced iNOS Overexpression in Bone Tissue

The impact of SPIO@PLGA and SPIO:Eu@PLGA nanospheres treatments on OVX-induced iNOS overexpression in bone tissue was evaluated through Western blot analysis, as illustrated in Figure 8a. Figure 8b demonstrates an elevated expression of iNOS, a key protein marker of M1 macrophages, in OVX femurs. Post-treatment with SPIO:Eu@PLGA nanospheres, a significant reduction in iNOS expression was observed, effectively reverting it to levels comparable to those in the sham group.

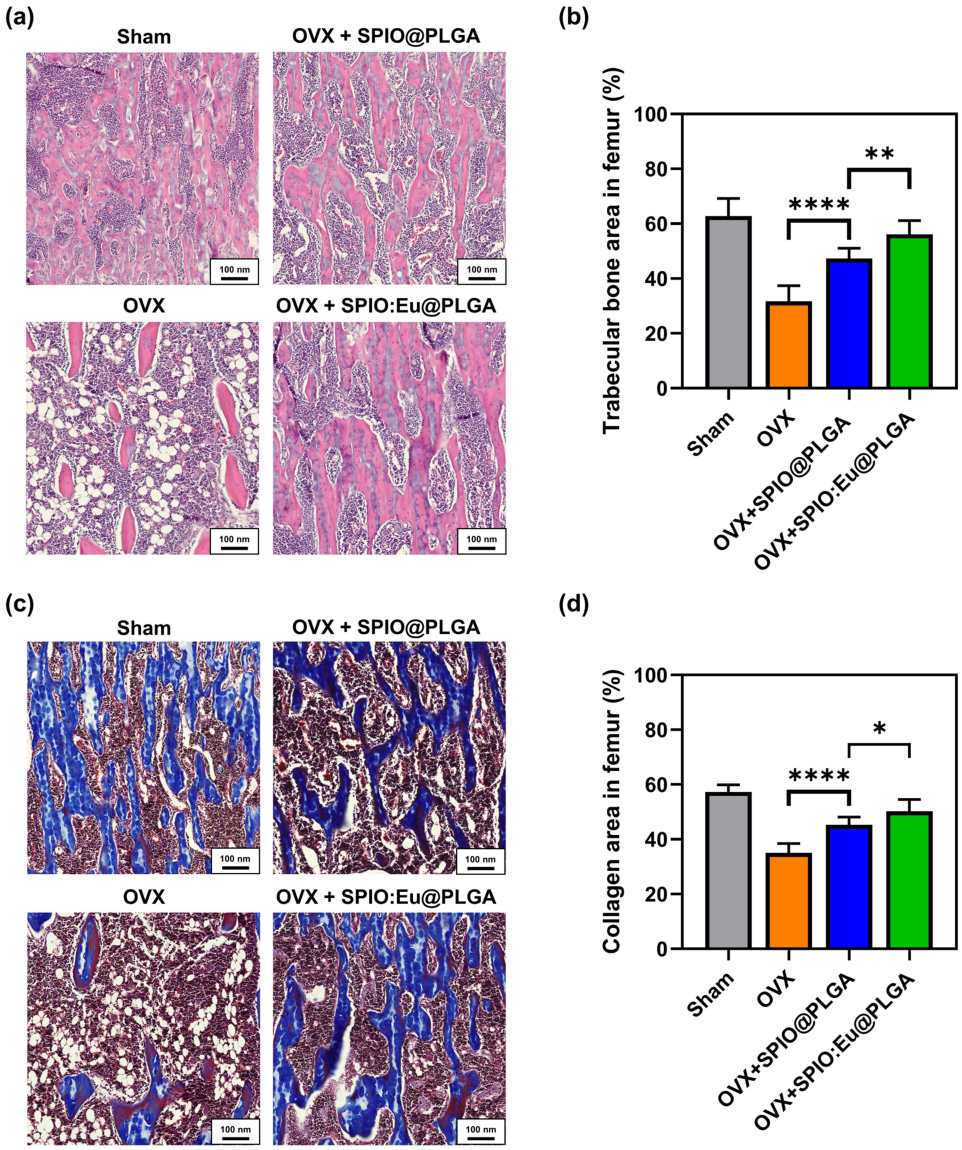

Figure 7 Effect of SPIO:Eu@PLGA nanospheres on preventing osteoporosis deterioration in ovariectomized (OVX) rats. (**a**) Histological examination using hematoxylin and eosin (HE) staining. (**b**) Quantitative analysis of trabecular area, identified in pink color, utilizing image data from panel (**a**), with subsequent statistical evaluation. (**c**) Determination of mineralized trabecular content through Goldner's trichrome staining, which distinguishes collagen in the mineralized bone matrix by blue color. (**d**) Quantitative assessment of the blue area using image data from panel (**c**), followed by statistical analysis. SPIO:Eu@PLGA nanospheres demonstrated remarkable efficacy in maintaining the integrity of trabecular bone in the femurs of OVX rats. ImageJ software was utilized for the quantitative measurements of the images presented in this figure. Scale bar: 100 μm. Data represent the mean ± standard deviation from triplicate biologically independent samples. Statistical analysis was performed using one-way ANOVA (*p<0.05, **p<0.01 and ****p<0.0001).

Discussion

Osteoporosis, characterized by brittle bones and a heightened risk of fractures, presents major public health challenges due to its high treatment costs and associated issues like disability and productivity loss.[30] Concerns about adverse and rebound effects from long-term use of antiresorptive or osteoanabolic drugs underscore the urgent need for novel osteoporosis treatments and a deeper understanding of bone metabolism.[31] In our research, we introduce a nanocomplex designed to target osteoporosis sites precisely, incorporating components that regulate ROS and promote bone formation. This approach leverages SPIO nanocrystals as a delivery mechanism, doped with osteogenic elements (Eu ions) to harness both magnetism-assisted targeting, ROS modulation and osteogenesis for direct action at sites of bone degeneration. To optimize IV administration, we embedded Eu-doped SPIO nanocrystals in PLGA, thereby forming SPIO:Eu@PLGA nanospheres. As illustrated in Figure 1, despite the introduction of Eu leading to a change in the

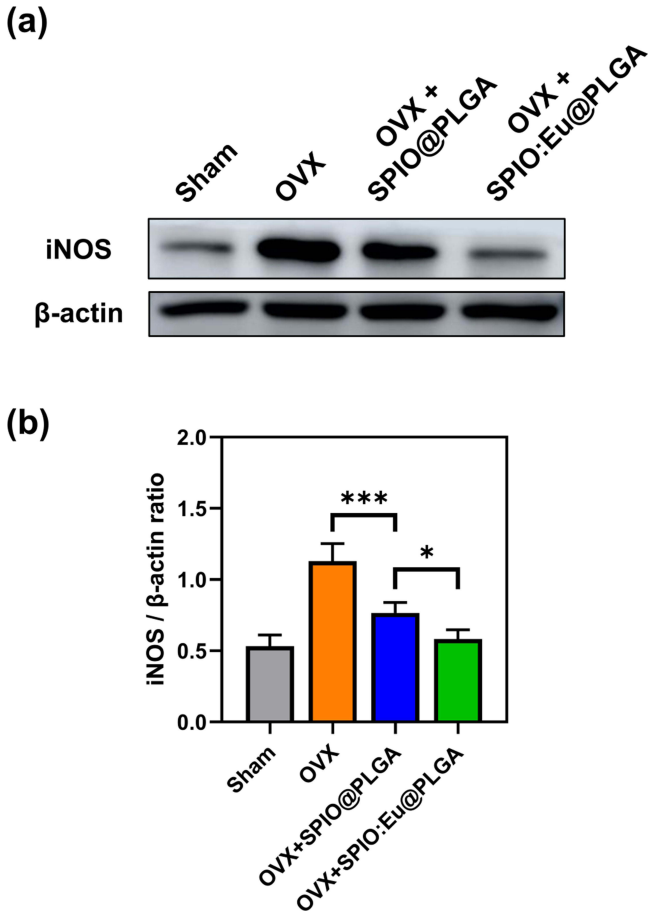

Figure 8 Effect of SPIO@PLGA and SPIO:Eu@PLGA nanospheres treatments on OVX-induced inducible nitric oxide synthase (iNOS) overexpression in bone tissue. (**a**) Characterization of iNOS through Western blot analysis. (**b**) Quantitative and statistical analysis of the results depicted in panel (**a**). Remarkably, iNOS, a key protein marker of M1 macrophages, exhibited an elevated expression in OVX femurs. Post-treatment with SPIO:Eu@PLGA nanospheres, a substantial reduction in iNOS expression was observed, effectively restoring it to levels comparable to those in the sham group. Data represent the mean ± standard deviation from triplicate biologically independent samples. Statistical analysis was conducted using one-way ANOVA, with significance levels denoted as *$p < 0.05$ and ***$p < 0.001$.

morphology of SPIO nanocrystals—potentially due to Eu ions altering the preferred growth direction of the SPIO crystal—the crystal structure (phase) remained unchanged after Eu doping and subsequent encapsulation in PLGA. This suggests that while Eu doping influences the shape of SPIO nanocrystals by modifying their crystal growth patterns, it does not affect the integrity of their crystal structure, as confirmed by the XRD analysis presented in Figure 1e. Additionally, XPS analysis further verified the successful incorporation of Eu into the SPIO nanocrystals (Figure S1). Both SPIO@PLGA and SPIO:Eu@PLGA nanospheres consistently measured at 90±10 nm in size. While SPIO is an FDA-approved MRI contrast agent and PLGA is an FDA-approved implant material, the cytotoxicity of SPIO:Eu@PLGA nanospheres had yet to be determined. To assess this, we evaluated the cytotoxicity of SPIO@PLGA and SPIO:Eu@PLGA nanospheres on MC3T3-E1 cell lines, which are murine calvarial pre-osteoblasts, and RAW264.7 cell lines, extensively used in studies of osteoclastic differentiation, molecular mechanisms, and macrophage polarization. Remarkably, even at a high concentration of 1000 μg/mL, our nanospheres exhibited no significant toxicity towards both MC3T3-E1 and RAW264.7 cells, as shown in Figure 2. Similar results were observed in hemocompatibility tests, confirming that neither SPIO@PLGA nor SPIO:Eu@PLGA nanospheres induced hemolysis, even at the same high concentration (Figure S2).

Macrophages are important in bone remodeling.[32] Recent study revealed that osteal macrophages increased and frequently located near osteoclasts on both trabecular and endocortical bone of OVX mice and in vitro study demonstrated a role for macrophages in facilitating osteoclastic bone resorption by engaging in phagocytosis and sequestering resorption byproducts.[11] Macrophage activation is dynamic. Hence, the concept of macrophage polarization is commonly

employed to highlight the activation status of macrophages at a specific location and time.[33] Various macrophage activation phenotypes exist, such as M1 macrophages, which emerge in inflammatory environments driven by Toll-like receptor (TLR) and interferon signaling. M2 macrophages are found in settings dominated by TH2 responses.

The classical macrophages activation is induced by lipopolysaccharide (LPS), a TLR agonist, and IFN-γ. Classically activated macrophages are often called M1. M1 macrophages are known not only for contributing to increased bone resorption through the secretion of pro-inflammatory cytokines but also for serving as precursors to osteoclasts.[34] A study found that estrogen deficiency-induced osteoclastogenesis in M2 macrophages results in an increased M1/M2 ratio in OVX mice.[15] Lowering the M1/M2 ratio represents a potential therapeutic approach for managing postmenopausal osteoporosis. In our research, which focused on the influence of nanospheres on macrophage polarization using the classical in vitro activation of mouse RAW264.7 macrophages with LPS, we observed a significant reduction in the activation of M1 ($CD11c^+$) macrophages following LPS stimulation with SPIO:Eu@PLGA nanospheres, as shown in Figure 3a and c. Additionally, this treatment promoted a shift towards the activation of M2 ($CD163^+$) macrophages, illustrated in Figure 3b and d. Most notably, we observed a significant decrease in the M1/M2 ratio, indicative of a diminished osteoclast effect, in samples treated with SPIO:Eu@PLGA nanospheres (Figure 3e).

It is known that LPS induces ROS production by directly interaction with NADPH oxidase. High level of ROS not only increases M1 macrophages' phagocytic activities, but also acts as a second messenger to activate mitogen-activated protein kinase (MAPK) and NF-κB and increase iNOS and TNF-α which increase inflammatory response.[35] Therefore, the reduction in the activation of M1 ($CD11c^+$) macrophages following LPS stimulation by SPIO:Eu@PLGA nanospheres is elucidated by ROS production, as characterized by the flow cytometry analysis results presented in Figure 4. This analysis distinctly shows the significant impact of both SPIO@PLGA and SPIO:Eu@PLGA nanospheres on the levels of ROS in LPS-induced M1 macrophages. These results are in alignment with Liu's research, which highlights the role of SPIO nanocrystals in modulating pro-inflammatory signals via their ROS scavenging capabilities.[18,36] The process of inflammation, often characterized by an increase in ROS production that leads to macrophage activation, appears to be effectively regulated by the ROS scavenging abilities of these nanoparticles. This is clearly evidenced by the observed decrease in M1 macrophage polarization following treatment with SPIO@PLGA and SPIO:Eu@PLGA nanospheres, as illustrated in Figure 3. Further, the augmented ROS scavenging capability of SPIO:Eu@PLGA nanospheres, compared to that of SPIO@PLGA nanospheres, is ascribed to the inclusion of Eu ions. The integration of lanthanide cations such as Eu into ceria structures is known to increase oxygen vacancies, thereby enhancing their capacity to neutralize ROS.[37,38] This mechanism is likely responsible for the more effective reduction in intracellular ROS levels and the significant downregulation of p-NF-κB transcription levels observed with SPIO:Eu@PLGA nanospheres treatment. The markedly greater reduction in p-NF-κB levels by SPIO:Eu@PLGA nanospheres, correlating with its enhanced ROS scavenging efficiency, underscores the critical importance of nanoparticle composition in effectively diminishing M1 macrophages' activities.

Emerging evidence indicates that oxidative stress, often intensified with age and/or menopause, is further aggravated by a lack of estrogen. This escalation in ROS adversely affects bone homeostasis, primarily through the promotion of osteoclastogenesis and the suppression of osteoblastic activity, culminating in osteoporosis.[39,40] Research has demonstrated that ROS enhance RANKL-induced osteoclastogenesis by activating signaling pathways, including mitogen-activated protein kinases (MAPKs) and NF-κB, in osteoclastic lineage cells.[41,42] In this context, our study was directed towards assessing the impact of our nanospheres on RANKL-induced osteoclastogenesis using RAW264.7 cells. We observed that osteoclasts, typically characterized in vitro as TRAP staining positive multinucleated cells, exhibited a significant decrease in their numbers following treatment with SPIO-containing nanospheres, especially SPIO:Eu@PLGA nanospheres, as shown in Figure 5a and b. Furthermore, the F-actin rings, essential for osteoclast polarization on bone and for the degradation of the mineralized matrix, were conspicuously missing in cells treated with SPIO@PLGA and SPIO:Eu@PLGA nanospheres (Figure 5c). It is suggested that these effects are substantially due to the reduction in intracellular ROS and p-NF-κB as a consequence of treatment with SPIO:Eu@PLGA nanospheres (Figure 4). In parallel, we utilized MC3T3-E1 mouse pre-osteoblasts to investigate osteoblast differentiation and matrix mineralization in vitro. ALP activity, a pivotal biomarker of osteoblast function essential for bone matrix mineralization,[43,44] was notably increased on day 14 following treatment with SPIO:Eu@PLGA nanospheres, as

shown in Figure 6a. Bone mineralization, a critical process in new bone formation and mediated by osteoblasts, involves the incorporation of calcium phosphate nanocrystals into the organic bone matrix. This aspect was further assessed through Alizarin Red S staining of MC3T3-E1 cultures treated with our nanospheres. As depicted in Figure 6b, the treatment with SPIO:Eu@PLGA nanospheres resulted in a marked enhancement in bone mineralization, evidenced by intensified red staining after 21 days. Although Eu might initially impede osteoblast differentiation (day 7), similar to the effects observed with high calcium concentrations.[45] It is important to note that the Eu concentration in our SPIO:Eu@PLGA nanospheres formulation was well-tolerated by osteoblasts without inducing any adverse effects, as clearly demonstrated in Figure 6a. In summary, the SPIO:Eu@PLGA nanospheres treatment not only modestly promoted bone formation but also significantly impeded bone resorption.

In Figures 3–6, $Eu(CH_3COO)_3$ was used at an equivalent Eu ion concentration to that in SPIO:Eu@PLGA, acting as a comparison group. This setup was designed to validate the specific effects attributed to the incorporation of Eu ions into the SPIO nanocrystals. The comparison highlights that the beneficial effects observed are directly linked to the incorporation of Eu ions within the SPIO crystal matrix. It points out that free Eu ions released from $Eu(CH_3COO)_3$, when not integrated into the SPIO matrix, do not achieve the same level of effectiveness. This emphasizes the critical role of incorporating Eu ions into the matrix for achieving the desired therapeutic outcomes. The enhanced effectiveness of the SPIO:Eu@PLGA nanospheres treatment in reducing intracellular ROS levels can be attributed to the Eu ions-induced oxygen vacancy in the SPIO crystal, supporting the importance of Eu ions' integration for the observed benefits.[37,38,46]

In our comprehensive final assessment, we assessed the therapeutic efficacy of our nanospheres containing Eu-doped SPIO nanocrystals on osteoporosis using OVX rats. The localization of iron-containing SPIO nanocrystals was identified through Perls' Prussian Blue staining, which showed an accumulation of these particles in the bone marrow near trabecular bone surfaces (highlighted by arrows, Figure S3). Histological examination of femurs from these rats revealed contracted and perforated bone trabeculae with a loss of continuity, alongside a decrease in bone trabecular mass and an increase in bone marrow fat fraction, consistent with previous studies.[47] Utilizing ImageJ software for analysis under light microscopy, we found that SPIO:Eu@PLGA nanospheres substantially preserved trabecular bone in OVX rat femurs more effectively than SPIO@PLGA nanospheres (Figure 7a and b). Through Goldner's trichrome staining, we observed that the trabeculae in osteoporotic femurs not only suffered a reduction in quantity but also experienced a loss of their collagen content in the bone matrix, which was replaced by non-mineralized content on the surface and appeared empty in central areas. Interestingly, both SPIO:Eu@PLGA and SPIO@PLGA nanospheres treatments not only repaired trabecular bone mass but also restored its mineralized content (Figure 7c and d). Similar results were observed in the micro-CT images (Figure S4), which further demonstrated significant improvements in trabecular density, connectivity, and thickness in the SPIO:Eu@PLGA-treated group compared to the OVX and SPIO@PLGA groups. These findings confirm the superior efficacy of Eu-doped nanospheres in mitigating the loss of both trabecular quantity and quality in osteoporotic bone.

To delve deeper into the tissue-level mechanisms, we analyzed the expression of macrophage-related proteins. Notably, the iNOS protein, a marker of M1 macrophages, was elevated in OVX femurs. Post-treatment with SPIO:Eu@PLGA nanospheres, a significant decrease in iNOS expression was noted, returning to levels observed in the sham group (Figure 8a and b). This reduction suggests that SPIO:Eu@PLGA nanospheres mitigates OVX-induced trabecular bone loss by modulating macrophage polarization in vivo. This is supported by the in vitro findings presented in Figure 3, where SPIO:Eu@PLGA nanospheres effectively reduced the M1/M2 ratio, highlighting its potential as a therapeutic target in treating OVX-induced osteoporosis.

In conclusion, our study presents initial evidence that SPIO:Eu@PLGA nanospheres may open a new path for treating osteoporosis. This strategy, aiming to address the limitations and side effects of traditional therapies, involves targeted delivery to bone tissue, modulation of macrophage polarization, and enhancement of bone remodeling. The use of SPIO nanocrystals doped with Eu, which combine magnetic guidance with ROS scavenging properties, has demonstrated promising results in both in vitro and in vivo models. It is important to note that due to the well-established efficacy of SPIO in magnetic navigation,[48–50] and in adherence to the focus of our research and animal welfare considerations, a non-magnetic field group was not included in our animal experiments. This study highlights the crucial role of Eu

doping in enhancing the anti-osteoporotic effects of SPIO:Eu@PLGA nanospheres, showing its efficacy at both cellular and tissue levels in vitro and in vivo. However, caution is advised, as the SPIO:Eu@PLGA nanospheres, despite their demonstrated biocompatibility and positive impact on bone structure in osteoporosis models, are still in the early stages of development within a complex medical field. Extensive further studies are required to fully determine the long-term efficacy and safety profile of materials containing Eu. In addition, future applications in other modulating immune and inflammatory indications, such as osteoarthritis, are also worth exploring.

Conclusion

In summary, the results from this study provide strong evidence supporting the effectiveness of SPIO@PLGA and SPIO:Eu@PLGA nanospheres in modulating macrophage activation, primarily attributed to their ROS scavenging abilities. A crucial aspect of this research is the unique role of Eu ions when integrated into the SPIO matrix, which significantly contributes to the observed beneficial effects. This distinction underlines that free Eu ions, when not incorporated into the SPIO matrix, fail to achieve comparable results. This research highlights the significant impact of Eu doping in enhancing the anti-osteoporotic properties of SPIO:Eu@PLGA nanospheres, with demonstrated effectiveness at both cellular and tissue levels, applicable to in vitro and in vivo settings. The inclusion of Eu in these nanospheres presents a promising direction for developing advanced treatments for osteoporosis resulting from OVX.

Abbreviations

Eu, europium; SPIO, superparamagnetic iron oxide; PLGA, poly(lactic-co-glycolic acid); ROS, reactive oxygen species; OVX, ovariectomized; NF-κB, nuclear factor kappa-light-chain-enhancer of activated B cells; IV, intravenous; TEM, transmission electron microscopy; XRD, X-ray diffraction; LPS, lipopolysaccharides; ALP, alkaline phosphatase; TRAP, tartrate-resistant acid phosphatase; RANKL, receptor activator of nuclear factor kappa-B ligand; macrophage colony-stimulating factor, M-CSF; SD, Sprague-Dawley; iNOS, inducible nitric oxide synthase.

Acknowledgments

We are grateful to the National Science and Technology Council, Far Eastern Memorial Hospital and the Taipei City Government for their funding support. We also thank the National Yang Ming Chiao Tung (NYCU) Instrumentation Resource Center for providing instrument and technical support.

We express our appreciation to Chen-Wei Lai at NYCY for their valuable assistance with the immune assays and insightful contributions during the experimental phases of this study.

Author Contributions

Tse-Ying Liu and Mei-Hsiu Chen are the corresponding authors with equal contribution. All authors made a significant contribution to the work reported, whether that is in the conception, study design, execution, acquisition of data, analysis and interpretation, or in all these areas; took part in drafting, revising or critically reviewing the article; gave final approval of the version to be published; have agreed on the journal to which the article has been submitted; and agree to be accountable for all aspects of the work.

Funding

We are grateful to the National Science and Technology Council (NSTC 111-2221-E-A49-051-MY2, NSTC 111-2811-E-A49A-007-MY2, NSTC 111-2314-B-038-094, NSTC 113-2314-B-A49-065-MY3, NSTC 113-2811-B-A49A-029), the Far Eastern Memorial Hospital (FEMH-2024-C-013, FEMH-2024-C-057, FEMH-2023-C-081), and the Department of Health, Taipei City Government (11201-62-004, 11301-62-048) for financial support.

Disclosure

The author(s) report no conflicts of interest in this work.

References

1. Sambrook P, Cooper C. Osteoporosis. *Lancet*. 2006;367(9527):2010–2018. doi:10.1016/S0140-6736(06)68891-0
2. Riggs BL, Melton LJ III. Evidence for two distinct syndromes of involutional osteoporosis. *Am J Med*. 1983;75(6):899–901. doi:10.1016/0002-9343(83)90860-4
3. Sobh MM, Abdalbary M, Elnagar S, et al. Secondary osteoporosis and metabolic bone diseases. *J Clin Med*. 2022;11(9):2382.
4. Li H, Xiao Z, Quarles LD, Li W. Osteoporosis: mechanism, molecular target and current status on drug development. *Curr Med Chem*. 2021;28(8):1489–1507. doi:10.2174/1875533XMTA1hNTIy2
5. Song S, Guo Y, Yang Y, Fu D. Advances in pathogenesis and therapeutic strategies for osteoporosis. *Pharmacol Ther*. 2022;237:108168.
6. Khosla S, Hofbauer LC. Osteoporosis treatment: recent developments and ongoing challenges. *Lancet Diabetes Endocrinol*. 2017;5(11):898–907. doi:10.1016/S2213-8587(17)30188-2
7. Langdahl B, Ferrari S, Dempster DW. Bone modeling and remodeling: potential as therapeutic targets for the treatment of osteoporosis. *Ther Adv Musculoskel Dis*. 2016;8(6):225–235. doi:10.1177/1759720X16670154
8. McClung M, Harris ST, Miller PD, et al. Bisphosphonate therapy for osteoporosis: benefits, risks, and drug holiday. *Am j Med*. 2013;126(1):13–20. doi:10.1016/j.amjmed.2012.06.023
9. Li -Y-Y, Gao L-J, Zhang Y-X, et al. Bisphosphonates and risk of cancers: a systematic review and meta-analysis. *Br J Cancer*. 2020;123(10):1570–1581. doi:10.1038/s41416-020-01043-9
10. Krege JH, Gilsenan AW, Komacko JL, Kellier-Steele N. Teriparatide and osteosarcoma risk: history, science, elimination of boxed warning, and other label updates. *JBMR Plus*. 2022;6(9):e10665. doi:10.1002/jbm4.10665
11. Batoon L, Millard SM, Raggatt LJ, et al. Osteal macrophages support osteoclast-mediated resorption and contribute to bone pathology in a postmenopausal osteoporosis mouse model. *J Bone Miner Res*. 2021;36(11):2214–2228. doi:10.1002/jbmr.4413
12. Muñoz J, Akhavan NS, Mullins AP, Arjmandi BH. Macrophage polarization and osteoporosis: a review. *Nutrients*. 2020;12(10):2999. doi:10.3390/nu12102999
13. Chen S, Tao L, Zhu F, et al. BushenHuoxue decoction suppresses M1 macrophage polarization and prevents LPS induced inflammatory bone loss by activating AMPK pathway. *Heliyon*. 2023;9(5):e15583. doi:10.1016/j.heliyon.2023.e15583
14. Liu YC, Zou XB, Chai YF, Yao YM. Macrophage polarization in inflammatory diseases. *Int J Bio Sci*. 2014;10(5):520–529. doi:10.7150/ijbs.8879
15. Dou C, Ding N, Zhao C, et al. Estrogen deficiency-mediated M2 macrophage osteoclastogenesis contributes to M1/M2 ratio alteration in ovariectomized osteoporotic mice. *J Bone Min Res*. 2018;33(5):899–908. doi:10.1002/jbmr.3364
16. Wang W, Liu H, Liu T, Yang H, He F. Insights into the role of macrophage polarization in the pathogenesis of osteoporosis. *Oxid Med Cell Longev*. 2022;2022:2485959. doi:10.1155/2022/2485959
17. Saengruengrit C, Ritprajak P, Wanichwecharungruang S, et al. The combined magnetic field and iron oxide-PLGA composite particles: effective protein antigen delivery and immune stimulation in dendritic cells. *J Colloid Interface Sci*. 2018;520:101–111. doi:10.1016/j.jcis.2018.03.008
18. Chen Y, Zeng Z, Ying H, Wu C, Chen S. Superparamagnetic iron oxide nanoparticles attenuate lipopolysaccharide-induced inflammatory responses through modulation of toll-like receptor 4 expression. *J Appl Toxicol*. 2020;40(8):1067–1075. doi:10.1002/jat.3967
19. Grosse S, Stenvik J, Nilsen AM. Iron oxide nanoparticles modulate lipopolysaccharide-induced inflammatory responses in primary human monocytes. *Int J Nanomed*. 2016;11:4625–4642. doi:10.2147/IJN.S113425
20. Yang DH, Yang MY. The role of macrophage in the pathogenesis of osteoporosis. *Int J Mol Sci*. 2019;20(9):2093.
21. Liu M, Shu M, Yan J, et al. Luminescent net-like inorganic scaffolds with europium-doped hydroxyapatite for enhanced bone reconstruction. *Nanoscale*. 2021;13(2):1181–1194. doi:10.1039/D0NR05608A
22. Wu L, Yang F, Xue Y, et al. The biological functions of europium-containing biomaterials: a systematic review. *Mater Today Bio*. 2023;19:100595. doi:10.1016/j.mtbio.2023.100595
23. Nicolete R, Santos DF, Faccioli LH. The uptake of PLGA micro or nanoparticles by macrophages provokes distinct in vitro inflammatory response. *Int Immunopharmacol*. 2011;11(10):1557–1563. doi:10.1016/j.intimp.2011.05.014
24. Shuai C, Yang W, Feng P, Peng S, Pan H. Accelerated degradation of HAP/PLLA bone scaffold by PGA blending facilitates bioactivity and osteoconductivity. *Bioact Mater*. 2021;6(2):490–502. doi:10.1016/j.bioactmat.2020.09.001
25. Feng P, Wu P, Gao C, et al. A multimaterial scaffold with tunable properties: toward bone tissue repair. *Adv Sci*. 2018;5(6):1700817. doi:10.1002/advs.201700817
26. Park J, An K, Hwang Y, et al. Ultra-large-scale syntheses of monodisperse nanocrystals. *Nature Mater*. 2004;3(12):891–895. doi:10.1038/nmat1251
27. Yang L, Zhou Z, Liu H, et al. Europium-engineered iron oxide nanocubes with high T1 and T2 contrast abilities for MRI in living subjects. *Nanoscale*. 2015;7(15):6843–6850. doi:10.1039/C5NR00774G
28. Guo Z, Shao L, Du Q, Park KS, Geller DA. Identification of a classic cytokine-induced enhancer upstream in the human iNOS promoter. *FASEB J*. 2007;21(2):535–542. doi:10.1096/fj.06-6739com
29. Morgan MJ, Liu ZG. Crosstalk of reactive oxygen species and NF-κB signaling. *Cell Res*. 2011;21(1):103–115. doi:10.1038/cr.2010.178
30. Rashki Kemmak A, Rezapour A, Jahangiri R, Nikjoo S, Farabi H, Soleimanpour S. Economic burden of osteoporosis in the world: a systematic review. *Med J Islamic Republic Iran*. 2020;34:154. doi:10.34171/mjiri.34.154
31. Foessl I, Dimai HP, Obermayer-Pietsch B. Long-term and sequential treatment for osteoporosis. *Nat Rev Endocrinol*. 2023;19(9):520–533. doi:10.1038/s41574-023-00866-9
32. Weivoda MM, Bradley EW. Macrophages and bone remodeling. *J Bone Min Res*. 2023;38(3):359–369. doi:10.1002/jbmr.4773
33. Murray PJ. Macrophage polarization. *Ann Rev Physiol*. 2017;79:541–566. doi:10.1146/annurev-physiol-022516-034339
34. Lassus J, Salo J, Jiranek WA, et al. Macrophage activation results in bone resorption. *Clin Orthopaedics Related Res*. 1998;352:7–15.
35. Tan HY, Wang N, Li S, Hong M, Wang X, Feng Y. The reactive oxygen species in macrophage polarization: reflecting its dual role in progression and treatment of human diseases. *Oxid Med Cell Longev*. 2016;2016:2795090. doi:10.1155/2016/2795090
36. Wu PC, Hsiao HT, Lin YC, Shieh DB, Liu YC. The analgesia efficiency of ultrasmall magnetic iron oxide nanoparticles in mice chronic inflammatory pain model. *Nanomedicine*. 2017;13(6):1975–1981. doi:10.1016/j.nano.2017.05.005
37. Kumar A, Babu S, Karakoti AS, Schulte A, Seal S. Luminescence properties of europium-doped cerium oxide nanoparticles: role of vacancy and oxidation states. *Langmuir*. 2009;25(18):10998–11007. doi:10.1021/la901298q

38. Gubernatorova EO, Liu X, Othman A, et al. Europium-doped cerium oxide nanoparticles limit reactive oxygen species formation and ameliorate intestinal ischemia–reperfusion injury. *Adv Healthcare Mater*. 2017;6(14):1700176. doi:10.1002/adhm.201700176
39. Kimball JS, Johnson JP, Carlson DA. Oxidative stress and osteoporosis. *J Bone Joint Surg Am Vol*. 2021;103(15):1451–1461. doi:10.2106/JBJS.20.00989
40. Iantomasi T, Romagnoli C, Palmini G, et al. Oxidative stress and inflammation in osteoporosis: molecular mechanisms involved and the relationship with microRNAs. *Int J Mol Sci*. 2023;24(4):3772. doi:10.3390/ijms24043772
41. Ashtar M, Tenshin H, Teramachi J, et al. The roles of ROS generation in RANKL-induced osteoclastogenesis: suppressive effects of febuxostat. *Cancers*. 2020;12(4):929. doi:10.3390/cancers12040929
42. Thummuri D, Naidu VGM, Chaudhari P. Carnosic acid attenuates RANKL-induced oxidative stress and osteoclastogenesis via induction of Nrf2 and suppression of NF-κB and MAPK signalling. *J Mol Med*. 2017;95(10):1065–1076. doi:10.1007/s00109-017-1553-1
43. Orimo H. The mechanism of mineralization and the role of alkaline phosphatase in health and disease. *J Nippon Med School*. 2010;77(1):4–12. doi:10.1272/jnms.77.4
44. Licini C, Vitale-Brovarone C, Mattioli-Belmonte M. Collagen and non-collagenous proteins molecular crosstalk in the pathophysiology of osteoporosis. *Cytokine Growth Factor Rev*. 2019;49:59–69. doi:10.1016/j.cytogfr.2019.09.001
45. Maeno S, Niki Y, Matsumoto H, et al. The effect of calcium ion concentration on osteoblast viability, proliferation and differentiation in monolayer and 3D culture. *Biomaterials*. 2005;26(23):4847–4855. doi:10.1016/j.biomaterials.2005.01.006
46. Shuai C, Shi X, Yang F, Tian H, Feng P. Oxygen vacancy boosting Fenton reaction in bone scaffold towards fighting bacterial infection. *Int J Extreme Manuf*. 2024;6(1):015101. doi:10.1088/2631-7990/ad01fd
47. Fazeli PK, Horowitz MC, MacDougald OA, et al. Marrow fat and bone--new perspectives. *J Clin Endocrinol Metab*. 2013;98(3):935–945. doi:10.1210/jc.2012-3634
48. Zhi D, Yang T, Yang J, Fu S, Zhang S. Targeting strategies for superparamagnetic iron oxide nanoparticles in cancer therapy. *Acta Biomater*. 2020;102:13–34. doi:10.1016/j.actbio.2019.11.027
49. Guo X, Li W, Luo L, et al. External magnetic field-enhanced chemo-photothermal combination tumor therapy via iron oxide nanoparticles. *ACS Appl Mater Interfaces*. 2017;9(19):16581–16593. doi:10.1021/acsami.6b16513
50. Liang Y-J, Wang H, Yu H, et al. Magnetic navigation helps PLGA drug loaded magnetic microspheres achieve precise chemoembolization and hyperthermia. *Colloids Surf A*. 2020;588:124364. doi:10.1016/j.colsurfa.2019.124364